# Intermolecular interactions of H$_2$S with rare gases from molecular beam scattering in the glory regime and from *ab initio* calculations

David Cappelletti[a)]
*Dipartimento di Ingegneria Civile ed Ambientale, Università di Perugia, 06100 Perugia, Italy*

Alessandra F. A. Vilela
*Instituto de Fisica, Universidade Brasilia, CP04455, Brasilia, DF, CEP 70919-970, Brazil*

Patricia R. P. Barreto
*Laboratório Associado de Plasma (LAP), Instituto Nacional de Pesquisas Espaciais (INPE)/MCT,
CP 515, São José dos Campos, São Paulo, CEP 1224 7-9 70, Brazil*

Ricardo Gargano
*Instituto de Fisica, Universidade Brasilia, CP04455, Brasilia, DF, CEP 70919-970, Brazil*

Fernando Pirani and Vincenzo Aquilanti
*Dipartimento di Chimica, Università di Perugia, 06100 Perugia, Italy*

Integral cross sections for collisions of rotationally hot H$_2$S molecules with rare gas atoms (Ne, Ar, and Kr) have been measured, in the collision energy range of 10–60 kJ mol$^{-1}$, using a molecular beam apparatus operating under high resolution both in angle and in velocity. A well resolved glory pattern has been measured which permitted the accurate characterization of the intermolecular potentials both at long range (in the attractive region) and at intermediate distances (in the well region). Considering the conditions used in the experiments, the obtained potentials must be considered very close to the spherical averages of the full intermolecular potential energy surfaces. Extensive *ab initio* calculations have also been carried out in parallel in order to characterize energy minima in the potential energy surfaces and energy barriers associated to the motion of the rare gas atoms around H$_2$S. An assessment of the relative role of the various interaction components has been also attempted: the combined analysis of experimental and theoretical results suggests that H$_2$S-rare gas aggregates are mainly bound by nearly isotropic noncovalent interactions of the van der Waals type. © *2006 American Institute of Physics*. [DOI: 10.1063/1.2218513]

## I. INTRODUCTION

Molecules containing an *X* atom with a high electron affinity, interacting with a rare gas atom (Rg) in the gas phase, are interesting prototypes for studying how intermolecular interactions, which are determined mainly by noncovalent forces, can be perturbed by charge transfer effects.[1] When *X* in the molecule is bound to hydrogen atoms the discussion is traditionally based on atomic electronegativities and the interaction of the *X*–H bond with a closed-shell partner is even more intriguing because of the possibility of the insurgency of a hydrogen bonded structure.[2] Indeed there is no "hydrogen bond force" in nature and a hydrogen bonded structure results from a delicate balance between the various components of the intermolecular interaction, whose partition in physically motivated terms is fundamental to shed light into the behavior of specific molecular aggregates. In particular, van der Waals (vdW) interactions, which include size repulsion (dominant at short intermolecular distances) and dispersion attraction (prevalent at large distances) can combine with induction and other additional contributions, whose strength can change with the nature of the interacting partners. How the relative role of these components varies from system to system serves to establish the grounds for a phenomenological approach.[1]

Recently, we demonstrated for the H$_2$O–Rg systems[3] that contributions to the interaction additional to vdW emerge at intermediate and short distances and play a role of increasing importance in going from He to Xe. We correlated the observed experimental effects to the formation of an embryonic hydrogen bonded structure.

In this work, we present a related study dealing with H$_2$S interacting with rare gas atoms. The S atom shows an electronegativity value $\sim$2.5 eV, to be compared with those of oxygen $\sim$3.5 eV and hydrogen $\sim$2 eV. Therefore, a "chemical" common sense would lead to think that any additional contribution to the vdW interaction should decrease of importance for H$_2$S with respect to H$_2$O; but is such an effect still measurable or negligible?

Only little experimental information is available in the literature, essentially on the H$_2$S–Ar complex, providing some information on the structure and internal dynamics. In particular, Viswanathan and Dyke[4] first reported the radio frequency and microwave spectrum of H$_2$S–Ar and its isotopomers, providing information on the complex geometry which resulted as having a nearly coplanar structure with the

[a)]Electronic mail: david.cappelletti@unipg.it

Ar lying in a direction orthogonal to the $C_{2v}$ symmetry axis of $H_2S$, at an effective distance of 0.398 nm. Further experimental work[5] has been devoted to a study of the microwave spectra of this complex characterizing more in detail the structure, essentially in agreement with the previous results, and its internal dynamics. *Ab initio* calculations at the Moller-Plesset (MP2) level, with correction for the basis set superposition errors, have been carried out for $Ar-H_2S$ (Ref. [6]) and a potential energy surface (PES), represented with an atom-atom additive pair scheme employing Lennard-Jones(12,6) functions, was fitted to the calculated points. Two equilibrium structures were identified and for their better characterization, correlated electron pair approximation (CEPA) and coupled cluster (CC) calculations were also performed. The equilibrium distances were located at 0.375 and 0.429 nm with a binding energy of the order of 1.8 kJ mol$^{-1}$. Similar calculations were performed by the same authors for $H_2S-Ne$ (Ref. [7]) finding an equilibrium distance of 0.352 nm with interaction energy of about 1.0 kJ mol$^{-1}$.

We faced the study of these systems performing (Sec. II) high resolution molecular beam scattering experiments in the glory regime with the purpose to obtain a characterization of the interaction potentials, both in the region of the minimum of the well and at long range. To this aim, a velocity selected $H_2S$ molecular beam has been scattered by Ne, Ar, and Kr gaseous targets, providing measurements of the total integral cross section as a function of the collision velocity. Quantum interference effects have been resolved, overimposed to the smooth component of the cross section, and effective averaged interaction potential energy curves have been determined from the fit of the experimental data (Secs. II and III). In parallel, calculations were carried out in Brasilia by *ab initio* methods (Sec. IV), with the purpose to define both the most stable geometry of each $H_2S-Rg$ complex (Rg=He, Ne, Ar, and Kr), and the energy barriers associated to the motion of Rg both in the plane and out of the plane of $H_2S$. In the analysis of the data it has also been kept into account of the predictive power of some correlation formulas,[8] defined in terms of the polarizabilities of the involved species. Section V presents a comparison among results of experiments, *ab initio* calculations, and phenomenological predictions. This will help to build up a unifying picture both with regards to the gradual change of the total interaction, passing from a system to another, and to define the role of possible additional components which can provide a stabilizing effect to the vdW interaction.

## II. DESCRIPTION OF THE EXPERIMENT

The apparatus is formed by a sequence of vacuum chambers where the molecular beam of $H_2S$ is produced, collimated, velocity selected, attenuated by a gaseous target (in this experiment a rare gas), and detected by a mass spectrometer. The molecular beam source has been operated in the range of low pressures ($P_0=4-10$ mbars) and the nozzle has been heated to around 600 K both to avoid cluster formation and to produce rotationally hot molecules. Velocity selection is provided by a mechanical device of eight rotating disks, that allows the sampling of narrow slices of the molecular beam velocity distribution with a full width at half maximum of $\sim 5\%$. The scattering chamber is filled (with the target gas) and evacuated with a period of about 20 s/cycle with the purpose of measuring the attenuation of the molecular beam intensity under reproducible conditions and to reduce any systematic error in the measurements. The walls of the chamber are cooled with liquid air, which is contained in a cryostat attached to the chamber itself, with the purpose of decreasing the thermal random motion of the target gas. The value of the product between the density of the gas and the length of the collision path, necessary to get the absolute value of the integral cross section $Q$ through the Lambert-Beer law, is obtained by using an opportune calibration procedure.[9] More details of the experimental techniques are reported elsewhere.[10]

## III. ANALYSIS OF THE SCATTERING EXPERIMENTS: THE PHENOMENOLOGICAL SPHERICAL INTERACTION

The measured integral cross section $Q(v)$ are reported in Fig. 1, as a function of the selected velocity $v$ of the $H_2S$ projectile molecules (scattered by Ne, Ar, and Kr targets).

In the velocity range of these experiments a quantum mechanical interference effect, the "glory," can be seen, so that $Q(v)$ can be represented as a sum of a smooth, $\bar{Q}$, and an oscillatory, $Q_{glory}$, components,[11]

$$Q = \bar{Q} + Q_{glory}.$$

The measurement of $\bar{Q}$, in an absolute scale, is a probe of long range attractive forces: for an effective potential $V(R)$ varying as $R^{-6}$ it can be shown to decrease, as a function of $v$, according to a $\bar{Q} \sim v^{-2/5}$ dependence.[11,12] The oscillating component $Q_{glory}$ leads to the characterization of $V(R)$ in the region of the potential well. The data in Fig. 1 are plotted as $Q(v) \times v^{2/5}$ to put into evidence the oscillatory structures of the glory quantum interference. Since the projectile molecules are rotationally hot and $Q(v)$ in the glory region is mainly determined by collisional events at large and intermediate impact parameters, inelastic events play a secondary role. Therefore for the analysis of the experimental data it is sufficient to take into account only elastic scattering.[13] As anticipated a heated source has been used here, providing a slightly hyperthermal molecular beam ($v \leqslant 2000$ m/s) containing rotationally hot $H_2S$ molecules. In these conditions it is reasonable to assume that during every collision the projectile molecules have sufficient time to mediate the effect of the orientation anisotropy and therefore from $Q(v)$ it is possible to extract information on the radial potential $V(R)$ (interaction averaged over possible relative orientations).

As in the past,[3,13,14] an appropriate parametric functional form for $V(R)$ was adopted in order to separate information coming from the fitting of the absolute value of $\bar{Q}$ and from the oscillating behaviour of $Q_{glory}$. The functional form of the potential, expressed scaling $R$ and $V(R)$, respectively, for location $R_m$ and depth $\varepsilon$ of the potential well, $x=R/R_m$ and $f(x)=V(R)/\varepsilon$, is the following:
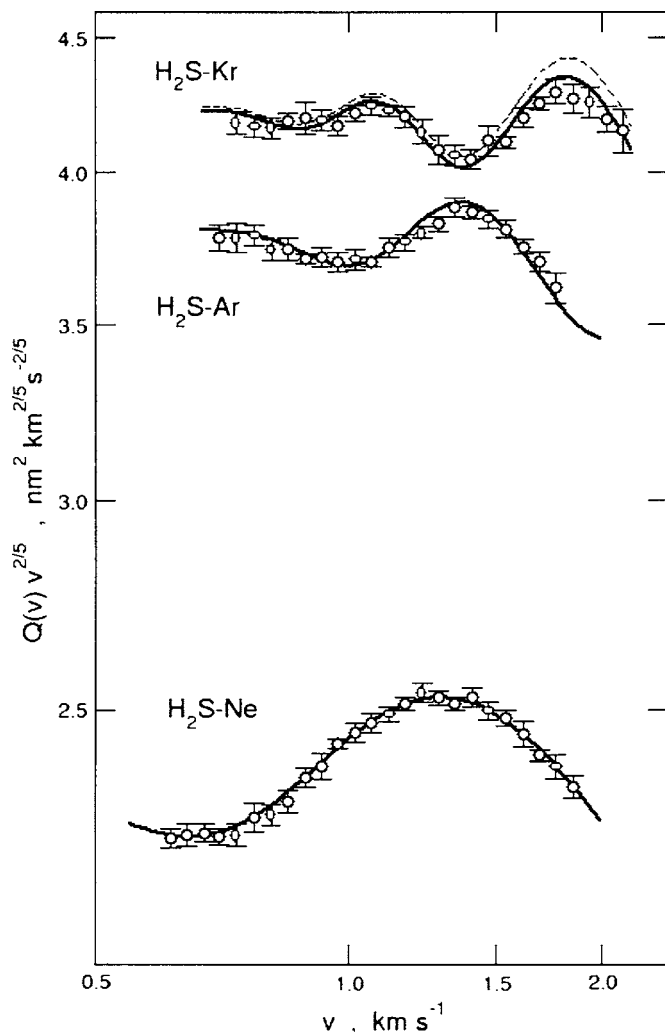
FIG. 1. Absolute integral cross section $Q$ for the scattering of H$_2$S by Ne, Ar, and Kr, as measured as a function of the H$_2$S molecular beam velocity $v$ and plotted as $Q(v) \times v^{2/5}$ (see text). Curves are calculated from best-fit interaction potentials of Fig. 2 and Table I. In the case of H$_2$S–Kr the dashed line is the cross section calculated without correction for the experimental angular resolution (see text).

$$f(x) = e^{-2\beta(x-1)} - 2\beta e^{-\beta(x-1)} \quad \text{for } x \leqslant x_1,$$

$$f(x) = b_1 + (x - x_1)b_2 + (x - x_2)[b_3 + (x - x_3)b_4]$$
$$\text{for } x_1 < x < x_2,$$

$$f(x) = -\frac{C_{LR}}{\varepsilon R_m^6} x^{-6} \quad \text{for } x_2 \leqslant x.$$

The $\beta$ parameter, which defines the curvature of the potential well, has been fixed at 6.5 for all systems, a value appropriate for noncovalent interactions between neutral closed-shell species,[8] $x_1$ and $x_2$ are chosen, as in previous cases, in the neighbourhood of 1.1 and 1.5 (specifically $x_1$ =1.12 and $x_2$=1.50), while $b_1$, $b_2$, $b_3$, and $b_4$—the spline parameters—are automatically fixed by imposing that the function must have the same value and the same derivative at $x_1$ and $x_2$. Final values are reported in Table I. For a given system, the analysis of the smooth component of the cross section, $\bar{Q}(v)$, yields direct information on the long range

TABLE I. Parameters for the H$_2$S–Rg spherical interaction as obtained from present experiments and correlation formulas (Ref. 8) (in italic). (Estimated experimental uncertainties are 5% for $\varepsilon$, 3% for $R_m$, and 8% for $C_{LR}$. Associated spline parameters $b_{1,\ldots}$, $b_4$ are −0.7067, 1.5484, −4.4188, and 4.1826, for H$_2$S–Ne; −0.7067, 1.5299, −4.4675, and 4.6339, for H$_2$S–Ar; −0.7067, 1.5621, −4.3827, and 3.8483, for H$_2$S–Kr).

|  | $R_m$ (nm) | $\varepsilon$ (kJ mol$^{-1}$) | $C_{LR}$ (kJ mol$^{-1}$ nm$^{-6}$) |
|---|---|---|---|
| H$_2$S–Ne | 0.391 | 0.520 | 25.1 |
|  | *0.389* | *0.527* | *25.4* |
| H$_2$S–Ar | 0.405 | 1.45 | 91.2 |
|  | *0.406* | *1.38* | *85.7* |
| H$_2$S–Kr | 0.415 | 1.86 | 123 |
|  | *0.415* | *1.79* | *127* |

effective interaction constant $C_{LR}$, defining the effective long range attraction $C_{LR} \times R^{-6}$ in a specific $R$ range,[12] while from the glory pattern the well depth $\varepsilon$ and its location $R_m$ are obtained by a trial-and-error procedure. The $R$ range of $C_{LR}$ validity is 0.56–0.65 nm for Ne, 0.69–0.82 nm for Ar, and 0.70–0.85 nm for Kr. The cross sections, calculated in the center of mass frame (CM) using a "fast and accurate semi-classical procedure,"[12] are convoluted in the laboratory system for a comparison with the experimental data. The convolution procedure includes both the average over the thermal motion of the target gas and the transmission function of the velocity selector. In the case of H$_2$S–Kr a small correction to the cross sections, the inherent error due to the finite angular resolution of the apparatus (the so called "limit angle" correction, due to the uncertainty principle) has been introduced in the calculation.[10,15] The dashed line in Fig. 1 represents the calculated cross sections without this correction, while the full line includes it. Such a correction, which depends on mass and velocity of the projectile, on the cross section value, and on the angular resolution of the experiment, is negligible for the scattering of H$_2$S by the other rare gases.
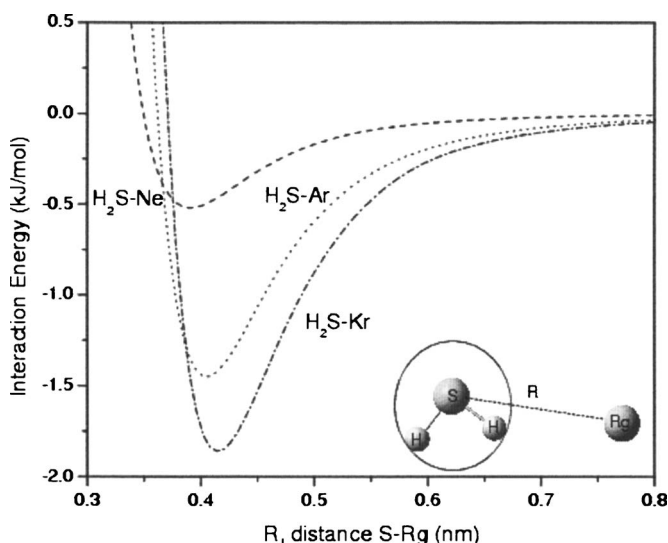


FIG. 2. Experimental averaged interaction potential curves for the H$_2$S–Ne, H$_2$S–Ar, and H$_2$S–Kr complexes, with parameters as in Table I and in the text.

TABLE II. Properties of $H_2S$ for different basis sets.

| Basis set | RS–H (nm) | $\theta$ | $\omega_1$ (cm$^{-1}$) | $\omega_2$ (cm$^{-1}$) | $\omega_3$ (cm$^{-1}$) | $\mu$ (D) | $\alpha$ (a.u.) |
|---|---|---|---|---|---|---|---|
| cc-pVDZ | 0.134 6 | 92.43 | 1213.64 | 2792.08 | 2516.55 | 1.2981 | 14.661 |
| cc-pVTZ | 0.133 5 | 92.25 | 1210.32 | 2781.47 | 2800.78 | 1.1560 | 18.241 |
| aug-cc-pVDZ | 0.134 9 | 92.43 | 1193.12 | 2754.84 | 2779.50 | 1.1374 | 23.592 |
| aug-cc-pVTZ | 0.133 6 | 92.22 | 1211.32 | 2772.85 | 2792.74 | 1.0911 | 24.377 |
| 6-311++G | 0.138 11 | 94.64 | 1196.06 | 2483.76 | 2514.93 | 1.8530 | 17.453 |
| 6-311++G($d,p$) | 0.133 4 | 92.07 | 1233.54 | 2815.46 | 2834.61 | 1.3649 | 17.891 |
| 6-311++G($2d,2p$) | 0.133 1 | 92.15 | 1229.12 | 2756.67 | 2774.86 | 1.1451 | 20.102 |
| 6-311++G($2df,2pd$) | 0.133 3 | 92.13 | 1221.11 | 2789.20 | 2799.33 | 1.1475 | 20.051 |
| 6-311++G($3d,3p$) | 0.133 2 | 92.36 | 1224.75 | 2784.93 | 2803.72 | 1.0640 | 23.182 |
| 6-311++G($3df,3pd$) | 0.133 2 | 92.30 | 1215.50 | 2790.34 | 2809.72 | 1.0610 | 23.015 |
| 6-311++G($3d2f,2p$) | 0.133 2 | 92.37 | 1223.67 | 2776.26 | 2795.26 | 1.0873 | 22.843 |
| 6-311++G($3d2f,3p2d$) | 0.133 2 | 92.17 | 1222.96 | 2782.55 | 2801.88 | 0.9791 | 23.197 |
| 6-311++G($3d2f,3p2d$) ($6d,10f$) | 0.133 2 | 92.16 | 1225.11 | 2784.30 | 2803.47 | 0.984 | 23.240 |
| Reference | 0.132 8 (Ref. [17]) | 92.2 (Ref. [17]) | 1183 (Ref. [18]) | 2615 (Ref. [18]) | 2626 (Ref. [18]) | 0.97 (Ref. [19]) | 25.5 (Ref. [20]) |

Figure 2 shows the experimental $V(R)$ curves and Table I reports the $\varepsilon$ and $R_m$ parameters and the $C_{LR}$ constant for each studied system, as obtained by the fitting procedure. The same table also shows the values predicted by correlation formulas,[8] which have been applied by taking into account for the polarizabilities $\alpha$ of $H_2S$ and of the rare gases and including also the effects due to the permanent dipole moment $\mu$ of $H_2S$ (see Tables II and III).

## IV. *AB INITIO* CALCULATIONS

To complete this study, extensive *ab initio* calculation were carried out, to determine both energy and structure of the $H_2S$–Rg complexes, with Rg=He, Ne, Ar, and Kr. These calculations were performed using the GAUSSIAN03 program.[16] The choice of the basis sets is the first issue, documented from calculations for the separated monomers ($H_2S$ and the four rare gases) in Tables II and III, and from preliminary optimization calculations on the equilibrium distance and binding energy of $H_2S$–Rg complexes, in Table IV. A total of 13 different basis sets were used at second-order MP2 level. Extensive calculations were also carried out at the CCSD(T) level and at the same geometries. Interaction energies were only slightly smaller than for MP2 (−13% for Kr, −6% for Ar, −17% for Ne, and −32% for He) and there-

TABLE III. Polarizability (in a.u.) of Rg atoms for different basis sets.

| Basis set | He MP2 | He QCISD(T) | Ne MP2 | Ne QCISD(T) | Ar MP2 | Ar QCISD(T) | Kr MP2 | Kr QCISD(T) |
|---|---|---|---|---|---|---|---|---|
| cc-pVDZ | 0.304 | ⋯ | 0.481 | 0.843 | 3.817 | 3.832 | 6.819 | 6.846 |
| cc-pVTZ | 0.636 | 0.6388 | 1.029 | 1.031 | 6.485 | 6.49 | 11.149 | 11.166 |
| aug-cc-pVDZ | 1.3376 | 1.3623 | 1.988 | 1.983 | 9.7617 | 9.839 | 14.549 | 14.672 |
| aug-cc-pVTZ | 1.3435 | 1.3669 | 2.437 | 2.425 | 10.813 | 10.844 | 16.645 | 16.729 |
| 6-311++G | 0.0 | 0.0 | 0.757 | 0.756 | 2.654 | 2.676 | 4.614 | 4.708 |
| 6-311++G($d,p$) | 0.633 | 0.635 | 1.015 | 1.013 | 4.993 | 5.054 | 10.472 | 10.529 |
| 6-311++G($2d,2p$) | 1.142 | 1.1577 | 1.406 | 1.402 | 7.520 | 7.559 | 15.007 | 15.142 |
| 6-311++G($2df,2pd$) | 1.145 | 1.1637 | 1.404 | 1.399 | 7.558 | 7.557 | 14.984 | 15.031 |
| 6-311++G($3d,3p$) | 1.347 | 1.3676 | 2.062 | 2.057 | 10.255 | 10.342 | 16.372 | 16.532 |
| 6-311++G($3df,3pd$) | 1.348 | 1.3713 | 2.058 | 2.05 | 10.242 | 10.263 | 16.308 | 16.355 |
| 6-311++G($3d2f,2p$) | 1.142 | 1.158 | 2.065 | 2.056 | 10.368 | 10.40 | 16.552 | 16.617 |
| 6-311++G($3d2f,3p2d$) | 1.354 | 1.379 | 2.065 | 2.057 | 10.367 | 10.401 | 16.552 | 16.618 |
| 6-311++G($3d2f,3p2d$) ($6d,10f$) | 1.354 | 1.378 | 2.068 | 2.058 | 10.390 | 10.426 | 16.676 | 16.749 |
| Reference | 1.383 (Ref. [21]) 1.3819 (Ref. [22]) 1.3833 (Ref. [23]) 1.3708 (Ref. [24]) | | 2.669 (Ref. [21]) 2.7272 (Ref. [24]) | | 11.08 (Ref. [21]) 11.1982 (Ref. [24]) | | 16.79 (Ref. [21]) 17.096 (Ref. [24]) | |

TABLE IV. Equilibrium distance $R_e$ (nm) and interaction energy $E_{CP}$ (in kJ/mol) for different basis sets.

| | H$_2$S−He | | H$_2$S−Ne | | H$_2$S−Ar | | H$_2$S−Kr | |
|---|---|---|---|---|---|---|---|---|
| | $R_e$ | $E_{CP}$ | $R_e$ | $E_{CP}$ | $R_e$ | $E_{CP}$ | $R_e$ | $E_{CP}$ |
| cc-pVDZ | 0.4192 | 0.0544 | 0.3856 | 0.0042 | 0.4487 | −0.2594 | 0.4577 | −0.4812 |
| cc-pVTZ | 0.4425 | −0.0753 | 0.4101 | −0.1046 | 0.4416 | −0.8661 | 0.4470 | −1.1171 |
| 6-311++G | 0.4850 | 0.0084 | 0.4350 | 0.2092 | 0.4481 | 0.2552 | 0.4817 | 0.1757 |
| 6-311++G($d,p$) | 0.4334 | −0.0418 | 0.4121 | 0.2803 | 0.4340 | 0.2176 | 0.4524 | −0.5063 |
| 6-311++G($2d,2p$) | 0.4237 | −0.1255 | 0.4030 | 0.0837 | 0.4381 | −0.7280 | 0.4452 | −1.0837 |
| 6-311++G($2df,2pd$) | 0.4134 | −0.1339 | 0.4022 | 0.0669 | 0.4334 | −0.8017 | 0.4385 | −1.1757 |
| 6-311++G($3d,3p$) | 0.4104 | −0.1213 | 0.4007 | −0.2427 | 0.4240 | −1.0293 | 0.4359 | −1.3054 |
| 6-311++G($3df,3pd$) | 0.4100 | −0.1297 | 0.3984 | −0.2427 | 0.4224 | −1.1506 | 0.4347 | −1.4937 |
| 6-311++G($3d2f,3p2d$) | 0.3480 | −0.2720 | 0.3900 | −0.4477 | 0.4120 | −1.3431 | 0.4280 | −1.7280 |
| 6-311++G($3d2f,3p2d$)($6d,10f$) | 0.4175 | −0.1674 | 0.4073 | −0.3305 | 0.4177 | −1.3138 | 0.4291 | −1.8200 |
| 6-311++G($3d2f,2p$) | 0.4276 | −0.1423 | 0.3989 | −0.1674 | 0.4246 | −1.1799 | 0.4386 | −1.5355 |
| aug-cc-pVTZ | | | 0.4011 | −0.3598 | 0.4208 | −1.4853 | 0.4191 | −1.6443 |
| aug-cc-pVTZ($6d,10f$) | | | 0.4017 | −0.3724 | 0.4216 | −1.5564 | 0.4161 | −1.6067 |
| aug-cc-pVDZ | | | 0.4146 | −0.2636 | 0.4252 | −0.9958 | 0.4295 | −1.0460 |

fore most of the calculations were done at the less time consuming MP2 level. Table IV compares the main interaction parameters, Rg⋯S equilibrium distance and interaction energy, obtained using the 13 basis sets. One can see that results using the 6-311++G($3d2f,3p2d$) basis set are of the correct magnitude and exhibit trends for the studied systems in agreement with the experimental data (see Table I). This basis set has been employed for the subsequent extensive calculations.

The complex was completely optimized on this basis set. The equilibrium distance, $R_{H–S}$, and angle, $\theta_{H–S–H}$, for the H$_2$S monomer in each complex are 0.1332 nm/92.31°, 0.1332 nm/92.23°, 0.1332 nm/92.15°, and 0.1332 nm/92.24° for He, Ne, Ar, and Kr, respectively. Differences between the two H–S bonds are on the fifth digits. These values for each complex are very close to the equilibrium geometry for the isolated H$_2$S, 0.1328 nm and 92.2°.[17]

The interaction energies are determined using the supermolecular approach, defined as the difference energy among that of the H$_2$S–Rg complexes and that of the two monomers H$_2$S and Rg. In order to eliminate the basis set superposition error (BSSE), the full "counterpoise" Boys and Bernardi method[25] was used. According to it, the energies of monomers are calculated using the same full basis set, and the interaction energy is then defined as

$$E_{CP} = E_{AB}(\chi_A + \chi_B) - [E_A(\chi_A + \chi_B) + E_B(\chi_A + \chi_B)],$$

where $\chi_A$ and $\chi_B$ are the basis sets of each monomer of the complex AB.

An ample set of more than 600 single potential energy points on the surface, for each complex, was calculated and analyzed: here the H$_2$S geometry parameters are kept frozen at the equilibrium position presented previously. Four different schemes were used to explore the topology of the PESs.

The first exploratory calculations involved the search for the minima in the surfaces. Optimization procedures provided planar structures for all the rare gas complexes, with values of the equilibrium H–S–Rg angle, $\theta_e$ (see Fig. 3), of 99°, 69°, 27°, and 14.3° for He, Ne, Ar, and Kr respectively.

The interaction energy profile as a function of interatomic S–Rg distance has been computed at $\theta_e$ for the H$_2$S–Rg complexes. Results are plotted in Fig. 3. Along the Rg series the binding energy increases by a factor of 2, 5.5, and 7 while the distance increases by 10.3%, 16.1%, and 22.2%, in going from He to Kr. Similar trends were observed for the H$_2$O–Rg complex,[3] for which the *ab initio* energies increased by a factor of 2.3, 6.4, and 7.8 and the distances increased by 3% 12%, and 15%.

In order to probe the anisotropy of the PES's we investigated the energies as a function of three different angles (see Figs. 4–6). The coordinate system is defined considering the S atom located at the origin, with the $C_{2v}$ symmetry axis of the H$_2$S molecule coinciding with the $X$ axis and the two hydrogen atoms lying in the $XY$ plane. The angle $\theta_1$ describes the rotation in the $XY$ plane, starting from the $C_{2v}$
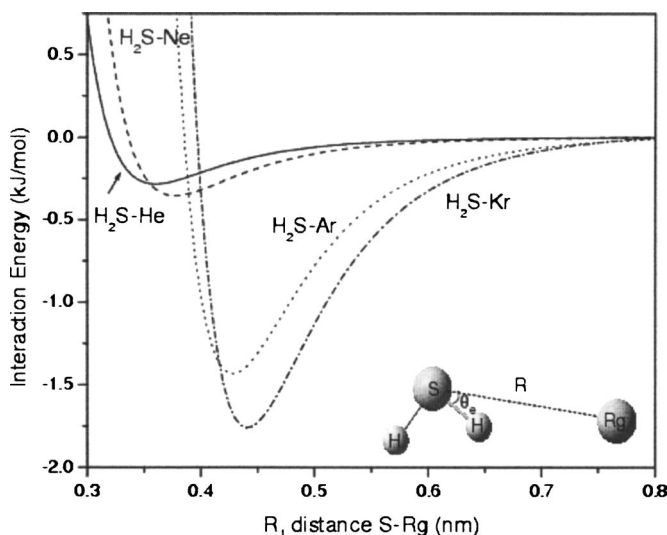


FIG. 3. Potential energy curves as a function of the S–Rg distance for the H$_2$S–Rg complexes with Rg=He, Ne, Ar, and Kr; computed at MP2/6-311++G($3d2f,3p2d$) including BSSE correction, at $\theta_e$ (see text). The H–S–Rg angle in the plane of the molecule, as obtained from an optimization calculation.

TABLE V. Geometric parameters of H$_2$S–Rg complexes calculated at the MP2 level with 6-311+
+G($3d2f$,$3p2d$) basis set.

| Complexes | $\theta_1$ [a] (degree) | $R_e$ (nm) Optimized | $R_e$ (nm) CP | $E$ (kJ mol$^{-1}$) Optimized | $E$ (kJ mol$^{-1}$) CP |
|---|---|---|---|---|---|
| H$_2$S–He | 106–254 | 0.348 | 0.360 | −0.272 | −0.286 |
| H$_2$S–Ne | 86–274 | 0.390 | 0.397 | −0.436 | −0.420 |
| H$_2$S–Ar | 0 | 0.412 | 0.418 | −1.343 | −1.611 |
| H$_2$S–Kr | 0 | 0.428 | 0.440 | −1.720 | −1.926 |

[a]For $\theta_2$=0 and $\theta_3$=90 (see Fig. 4).

symmetry axis; $\theta_2$ is the angle off of the molecular plane varying in the $XZ$ plane also starting from the $C_{2v}$ symmetry axis; $\theta_3$ describes the rotation in the $YZ$ plane, starting from the $Z$ axis. In the calculations for these three cases the S–Rg distance is kept constant at the value of equilibrium distance $R_e$ (see Table V) being 0.360, 0.397, 0.418, and 0.440 nm for He, Ne, Ar, and Kr, respectively.

The interaction energies as a function of $\theta_1$ are shown in Fig. 4. For all systems, maxima are found for the rare gas pointing along the S atom ($\theta_1$=180°) and symmetrically along the two H atoms ($\theta_1$=46° and 314°). Two symmetric absolute minima in the energy are found for He and Ne at angles $\theta_1$=106° (and 256°) and $\theta_1$=86° (and 274°) with energies of −0.286 and −0.460. The absolute minimum is found for Ar and Kr at $\theta_1$=0° (on the $C_{2v}$ axis) with energies of −1.611 and −1.926 kJ/mol, respectively. The binding energies, here, increase by a factor of 1.6, 5.6, and 6.7 in going from He to Kr, almost the same ratio observed before for the energy profile as function of Rg–S distance at $\theta_c$. The $\theta_1$ values corresponding to absolute minima are different from the less accurate ones from optimization ($\theta_e$ in Fig. 3), and the corresponding binding energy slightly higher. Note that for the case where discrepancy is larger, i.e., for Kr, it is nonetheless lower than a very small amount, 0.2 kJ/mol. In-

deed, barriers to free rotation in the plane are, e.g., within at most 0.5 kJ/mol for Kr, indicating a very low anisotropy of interaction.

In Fig. 5, we plot the interaction energies as a function of the $\theta_2$ angle. The minimum of the energy for all complexes is found at $\theta_2$=0°, confirming that these complexes are planar, with energies of −0.087, −0.420, −1.611, and −1.926 kJ/mol for He, Ne, Ar, and Kr, respectively. The minimum energy for Ar and Kr is the same as observed at $\theta_1$=0° while for the other Rg it is smaller.

The energy profile as a function of $\theta_3$ angle is presented in Fig. 6. The energy minima here are at $\theta_3$=90°, namely, in the molecular plane, for all complexes, and the curves are symmetric with respect to 180°.

Figures 4–6 demonstrate that the interaction energy anisotropy is small and comparable for all the systems. The energy barriers are always smaller than 0.5 kJ mol$^{-1}$, except for He moving along the $\theta_1$ coordinate where the barrier is about 1 kJ mol$^{-1}$. Most stable geometries appear to occur when the rare gases are in the molecular plane, consistently with previous studies[6,7] and with the analogous complexes of rare gases with H$_2$O.[3] However, more than one minimum energy geometry is observed: the smallness of the barriers separating them makes the assignment of the most stable configuration uncertain from the viewpoint of the accuracy
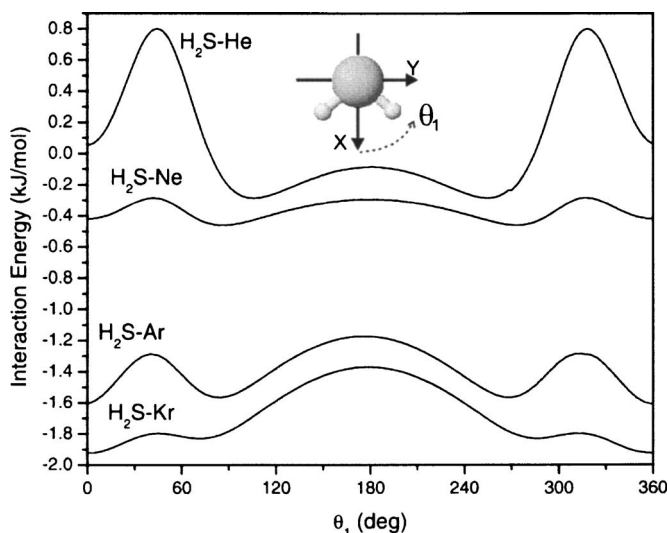


FIG. 4. Potential energy curves for the H$_2$S–Rg complexes as a function of the $\theta_1$ angle (see the inset), computed at MP2/6-311++G($3d2f$,$3p2d$) level including BSSE correction at the fixed distance $R_e$ (see Table V).



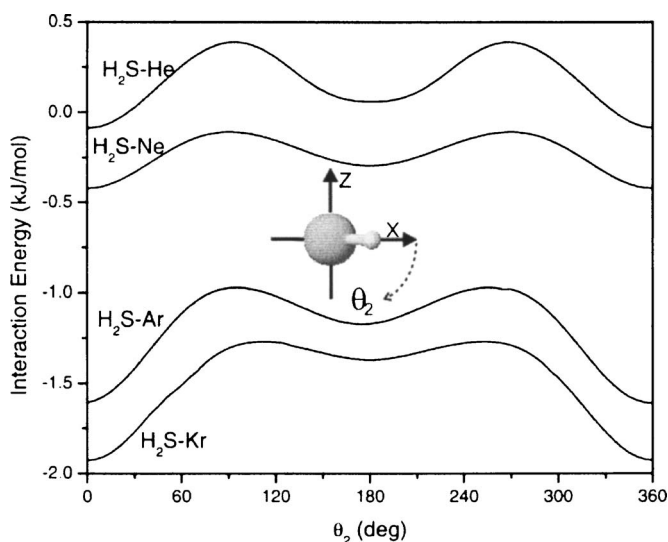FIG. 5. Potential energy curves for the H$_2$S–Rg complexes as a function of the $\theta_2$ angle (see Fig. 4).
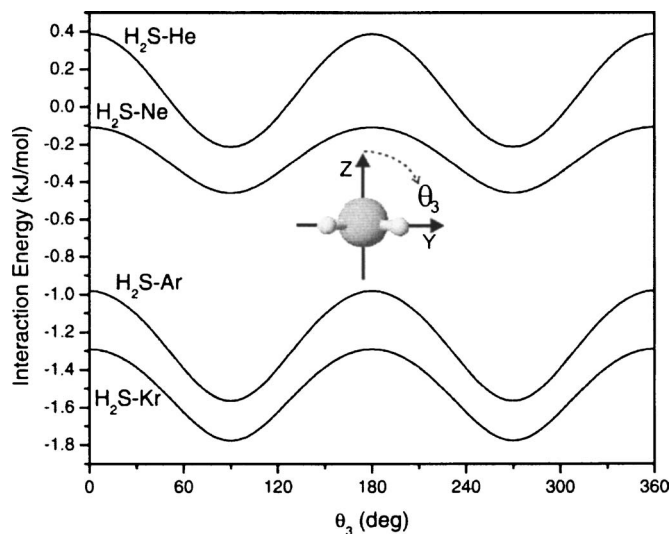
FIG. 6. Potential energy curves for the H$_2$S–Rg complexes as a function of the $\theta_3$ angle (see Fig. 4).

of the calculation. This is perhaps not relevant in view of the essential floppiness of these weakly bound systems, when zero point energy effects are taken into consideration.

Table V summarizes the calculated values, at the MP2 level, for the most stable configuration of all the complexes as obtained with and without the BSSE correction. The BSSE correction increases the equilibrium distance for all complexes analyzed. The values of H$_2$S–Ne and H$_2$S–Ar can also be compared with available theoretical data.[6,7] For the Ne case, the present *ab initio* calculations provide an equilibrium distance 10% larger and a binding energy more than a factor 2 less than the previous results.[7] For the Ar complex, the calculated equilibrium distance is in substantial agreement (within about 3%) with previous results[6] while the present calculated binding energy is 13% lower. Globally, the present calculations compare much better than previous results[6,7] with the experimental determinations ($R_m$ and $\varepsilon$) reported in Table I (considering $-\varepsilon \sim V_{\min}$). We did not deem necessary to obtain an averaged potential energy curve from the calculations and consider the above direct comparison of the most stable configuration with the experimental averaged curves sufficient because of the very small anisotropy of the PES.

## V. DISCUSSION

In this work we have experimentally characterized the intermolecular interaction potentials, which are operative in the weakly bound H$_2$S–Ne, H$_2$S–Ar, and H$_2$S–Kr aggregates. A molecular beam apparatus, operating under high resolution conditions in energy and angle, has been employed and the integral cross sections $Q$ have been measured in a wide range of collision velocity $v$. The scattering involved velocity selected rotationally hot H$_2$S projectile molecules, emerging from a heated molecular beam source, and rare gas atom targets (Ne, Ar, and Kr) confined into a liquid air cooled chamber. The used conditions are those appropriate to observe quantum interference effects in the scattering, such as the glory pattern in $Q(v)$. In fact, projectile molecules rotate sufficiently fast to minimize any quenching and shifting in the quantum interference effects[13] arising from anisotropy components in the intermolecular interaction potential. Therefore, the analysis of the measured $Q(v)$ provides $\varepsilon$ (well depth), $R_m$ (location of the well), and $C_{LR}$ (long range attraction coefficient) which are representative parameters of an effective interaction close to the spherical average of the potential energy surface. These results are important to experimentally establish, for the first time, the absolute scale of the binding energy, of the equilibrium distance, and of the long range attraction in the H$_2$S–Rg aggregates. For the H$_2$S–Ar system the determined $R_m$ value (0.405 nm) is in a very good agreement with the value of 0.398 nm, determined by spectroscopy.[4]

Theoretical calculations carried out at various levels and in parallel with the experiments, provided a set of complementary information. Specifically, they demonstrated that in the most stable geometries of all investigated systems the Rg atom lies in the plane of H$_2$S molecule. Several relative minima in the intermolecular potential energy have been localized and barriers between them characterized. All these features relate to in-plane and out-of-plane motions of the Rg atom, keeping fixed the intermolecular distance $R$. Such calculations also demonstrated that the barrier heights are in general small and of the same magnitude order or smaller of the binding energy in the most stable geometries. Globally, the potential energy surfaces look quite isotropic and this probably depends on the near symmetric electronic charge distribution around the H$_2$S molecule. Further calculations (here not reported and available on request) showed that pronounced modifications of the small barriers are observable when $R$ varies. However, they confirmed, in agreement with previous studies on H$_2$S–Ar,[6] that nearly isoenergetic and isotropic pathways describe the orbiting of Rg around H$_2$S. For these reasons it has not been possible to assign a most stable configuration for these complexes.

Combining information coming from present experiments and from the reported theoretical calculations, it can be inferred that the binding energy increases by about a factor 6, in going from H$_2$S–He to H$_2$S–Kr system. This work also shows that previous theoretical studies had overestimated the binding energy of about 13% for H$_2$S–Ar (Ref. 6) and of about of a factor 2 for H$_2$S–Ne.[7]

A further important effort has been focused on the understanding of the nature of the involved intermolecular potential, i.e., on the relative role of the basic components of the interactions, mainly affecting the intermolecular noncovalent bond in H$_2$S–Rg aggregates. Some predictions, concerning the basic intermolecular potential features $\varepsilon$, $R_m$, and $C_{LR}$, have been obtained considering the combined effect of vdW and induction components. The vdW features have been anticipated by using correlation formulas,[8] given in terms of polarizability values (the basic property controlling the vdW component) of the involved partners. Corrections due to the role of the induction have been also included. Note that the induction, arising from the permanent dipole-induced dipole interaction and here depending on the permanent dipole of H$_2$S (about on half of that of water) and on the polarizability of Rg, provides an increase of about 2.5% of

the attraction with respect to the pure dispersion.[3] Anyway its effect has been included in the evaluation. Predicted $\varepsilon$, $R_m$, and $C_{LR}$ potential parameters are compared in Table I with those obtained from the analysis of measured $Q(v)$. The good agreement suggests that in the present systems vdW and induction components basically control the intermolecular interaction potential energy. Other components (essentially electrostatic and charge transfer), relevant for the formation of a hydrogen bond,[2] are absent or not measurable. The satisfactory comparison with the parameters for the experimentally studied $H_2S-Ne$, $H_2S-Ar$, and $H_2S-Kr$ systems allows to safely extend the empirical evaluation of the same quantities for the $H_2S-He$ and $H_2S-Xe$ cases, not measured experimentally. The $\varepsilon$, $R_m$, and $C_{LR}$ parameters read 0.247 kJ $mol^{-1}$, 0.388 nm, and 11.7 kJ $mol^{-1}$ $nm^{-6}$ for He and 2.21 kJ $mol^{-1}$, 0.428 nm, and 191 kJ $mol^{-1}$ $nm^{-6}$ for Xe.

In conclusion, the combination of high resolution experiments with *ab initio* calculations and predictions of empirical correlation formulas sheds light on binding energy, energy barriers, anisotropy of the PES, and on the relative role of the leading interaction components operative in the $H_2S-Rg$ aggregates. This information is crucial to amplify the phenomenology of non covalent intermolecular interactions, especially to establish when additional components, relevant for the formation of the hydrogen bond, enter into play.[3]

## ACKNOWLEDGMENTS

[1] F. Pirani, G. Maciel, D. Cappelletti, and V. Aquilanti, Int. Rev. Phys. Chem. **25**, 165 (2006).

[2] See, for example, G. R. Desiraju and T. Steiner, *The Weak Hydrogen Bond in Structural Chemistry and Biology* (Oxford University Press, New York, 1999).

[3] V. Aquilanti, E. Cornicchi, M. M. Teixidor, N. Saendig, F. Pirani, and D. Cappelletti, Angew. Chem., Int. Ed. **44**, 2356 (2005); D. Cappelletti, V. Aquilanti, E. Cornicchi, M. M. Teixidor, and F. Pirani, J. Chem. Phys. **123**, 024302 (2005).

[4] R. Viswanathan and T. R. Dyke, J. Chem. Phys. **82**, 1674 (1985).

[5] R. E. Bumgarner, D. J. Pauley, and S. G. Kukolich, J. Mol. Struct. **190**, 163 (1988); H. S. Gutowsky, T. Emilsson, and E. Arunan, J. Chem. Phys. **106**, 5309 (1997).

[6] G. de Oliveira and C. E. Dykstra, J. Chem. Phys. **106**, 5316 (1997).

[7] G. de Oliveira and C. E. Dykstra, J. Chem. Phys. **110**, 289 (1999).

[8] R. Cambi, D. Cappelletti, G. Liuti, and F. Pirani, J. Chem. Phys. **95**, 1852 (1991); V. Aquilanti, D. Cappelletti, and F. Pirani, Chem. Phys. **209**, 299 (1996).

[9] T. Nenner, H. Tien, and J. B. Fenn, J. Chem. Phys. **63**, 5439 (1975); F. Pirani and F. Vecchiocattivi, *ibid.* **66**, 372 (1977).

[10] D. Cappelletti, M. Bartolomei, F. Pirani, and V. Aquilanti, J. Phys. Chem. A **106**, 10764 (2002).

[11] R. B. Bernstein and T. J. O'Brien, Discuss. Faraday Soc. **40**, 35 (1965); R. B. Bernstein and R. A. La Budde, J. Chem. Phys. **58**, 1109 (1973).

[12] F. Pirani and F. Vecchiocattivi, Mol. Phys. **45**, 1003 (1982).

[13] V. Aquilanti, D. Ascenzi, D. Cappelletti, M. de Castro, and F. Pirani, J. Chem. Phys. **109**, 3898 (1998).

[14] It is appropriate to note, as pointed out by one of the referees, that this potential function first appeared in one early paper, P. E. Siska, J. M. Parson, T. P. Schafer, and Y. T. Lee, J. Chem. Phys. **55**, 5762 (1971).

[15] V. Aquilanti, D. Ascenzi, E. Braca, D. Cappelletti, G. Liuti, E. Luzzatti, and F. Pirani, J. Phys. Chem. **101**, 6523 (1997).

[16] M. J. Frisch, G. W. Trucks, H. B. Schlegel *et al.*, GAUSSIAN 03, Revision C.02, Gaussian, Inc., Pittsburgh, 2003.

[17] G. Herzberg, *Electronic Spectra and Electronic Structure of Polyatomic Molecules* (Van Nostrand, New York, 1966).

[18] R. D. Nelson, Jr., D. R. Lide, and A. A. Maryott, *Selected Values of Electric Dipole Moments for Molecules in the Gas Phase* (National Bureau of Standards, Washington, 1967).

[19] T. Shimanouchi, *Tables of Molecular Vibrational Frequencies* (National Bureau of Standards, Washington, 1972).

[20] T. N. Olney, N. M. Cann, G. Cooper, and C. E. Brion, Chem. Phys. **223**, 59 (1997).

[21] T. M. Miller and B. Bederson, Adv. At. Mol. Phys. **13**, 1 (1984).

[22] Z. C. Yan, J. F. Babb, A. Dalgarno, and G. W. F. Drake, Phys. Rev. A **54**, 2824 (1996).

[23] J. Mitroy and M. W. J. Bromley, Phys. Rev. A **68**, 035201 (2003).

[24] G. Maroulis and A. Haskopoulos, Chem. Phys. Lett. **349**, 335 (2001).

[25] S. F. Boys and F. Bernardi, Mol. Phys. **19**, 533 (1970).